

## High beta plasma in improved confinement regime on the TPE-RX reversed-field pinch plasmas

H. Koguchi 1), H. Sakakita 1), Y. Hirano 1), K. Yambe 1), L. Frassinetti 1), F. Auriemma 2), D. Terranova 2), P. Innocente 2), S. Kiyama 1), and T. Shimada 1)

1) National Inst. of Advanced Industrial Science and Tech. (AIST), Tsukuba 305-8568, Japan

2) Consorzio RFX, I-35127 Padua, Italy

e-mail contact of main author: [h-koguchi@aist.go.jp](mailto:h-koguchi@aist.go.jp)

**Abstract.** A very high poloidal beta was achieved by the Pulsed Poloidal Current Drive (PPCD) in Toroidal Pinch Experiment-RX (TPE-RX, which had been operated to March 2007 from April 1998). The electron density and temperature increased, hence, the poloidal beta was improved to 30% from 5% during PPCD (poloidal beta is almost equal to total beta in the reversed-field pinch). D-alpha emission decreased during the PPCD and the ratio of the total number of particles to the D-alpha emission increased ten-fold at the end of the PPCD indicating the considerable improvement of the particle confinement time. Fast magnetic fluctuation levels in the edge region of TPE-RX were measured using a newly developed complex edge probe installed inside vacuum vessel and sensitive to fast magnetic fluctuation. During the PPCD operation, the magnetic fluctuation associated with the dynamo effect is reduced, and improved confinement is reached, which results in this high beta value. Unique neutral beam injection (NBI) system suitable for the RFP machine was developed to control plasma parameters. In the case of high power NB injection to the improved confinement plasma which was attained by PPCD operation with an ice pellet injection, the meaningful increments in the soft X-ray signal and the plasma current were found.

### 1. Introduction

Toroidal pinch experiment-RX (TPE-RX) was one of the largest reversed field pinch (RFP) devices in the world. The major radius  $R$  and minor radius  $a$  are 1.72 m and 0.45 m, respectively [1]. The operated maximum plasma current is 450 kA and achievable pulse length is 100 ms. In a standard discharge of TPE-RX the gas is fuelled by a steady flow of deuterium, and a pinch parameter,  $\Theta$  is controlled at the range 1.4-1.5. Here, the pinch parameter is one of the controlling parameters of RFP plasma, and is defined as a ratio of poloidal magnetic field at the plasma surface to averaged toroidal magnetic field ( $\Theta = B_{pa}/\langle B_t \rangle$ ). Global confinement properties under the standard discharge gives the range of poloidal beta,  $\beta_p = 5-10\%$ . The  $\beta_p$  is almost equal to the total beta in the RFP. The plasma density is almost proportional to the plasma current in the standard discharges, and is about  $5 \times 10^{18} \text{ m}^{-3}$  at the 300 kA of the plasma current. We applied several kinds of techniques in order to obtain highly improved confinement discharges. The confinement properties are generally limited by the core magnetic stochasticity generated by the core resonant tearing mode. Tearing mode are stabilized and magnetic stochasticity are reduced by applying the pulsed poloidal current drive (PPCD). The PPCD achieves high temperature and high  $\beta_p$  operation [2, 3]. The achievable electron temperature at the plasma center increases to a value three times higher than the standard discharge and reaches over 1.5 keV. The particle transport is reduced and the plasma electron density increases up to two times higher than the standard discharge. The  $\beta_p$  estimated from the electron temperature becomes very high. The mechanism of the ion heating during the PPCD is not clear and the ion heating is generally lower than the electron heating. The  $\beta_p$  value becomes 30% when the measured ion temperature is considered. A complex edge probe (CEP) was installed inside of the vacuum vessel ( $r/a = 1.00 \sim 1.08$ ). The CEP is composed of six pins that measure the floating potentials and of three magnetic sensor coils that can measure the toroidal, poloidal, and radial magnetic fields from 5 kHz to 10 MHz frequency bandwidth. The fast component of the magnetic

## EX/P5-25

fluctuation can be observed. We show that the increase in the particle confinement time,  $\tau_p$  is well correlated with the change in the nature of both the magnetic and the electrostatic turbulence measured by the CEP [4, 5]. In the TPE-RX device, standard RFP plasmas were characterized by magnetic and electrostatic edge turbulences having the strong intermittency. While in the improved confinement regime (ICR, whose definition will be given in the next chapter,) obtained by the PPCD, the edge turbulences have low intermittency but strong self-similarity [5].

NBI experiment was conducted during the PPCD with an ice pellet injection. This is the first result of high-power ( $>1\text{MW}$ ) and long-pulse ( $>30\text{ms}$ ) neutral beam (up to  $1.2\text{MW}$ ) injection experiment on the RFP. We injected the pellet into the PPCD plasma in order to reduce the orbit loss and the shine through by the increase of plasma density. The meaningful effects of the NBI are observed on the plasma current and on soft X-ray signal only in this case.

## 2. Pulsed Poloidal Current Drive

The PPCD operation is one of the improved confinement operations in RFP. The PPCD has been investigated in many RFP devices [6-9] and has become an extremely powerful technique since its first introduction in MST [6]. The PPCD is the method of generating the poloidal one-turn voltage directly by controlling external field coil current and of reducing the dynamo-effect. The external field coil is controlled in order to keep the electric field parallel to the magnetic field at the plasma surface ( $E_{\parallel}$ ) being positive. The  $E_{\parallel}$  is estimated from following equation,

$$E_{\parallel} = -E(a) \cdot B(a) / |B(a)| = [(V_{ta}/2\pi R)B_{ta} + (V_{pa}/2\pi a)B_{pa}] / (B_{ta}^2 + B_{pa}^2)^{1/2}.$$

Here,  $E(a)$  is electric field at the plasma surface,  $V_{ta}$  and  $V_{pa}$  is toroidal and poloidal one-turn voltage at the plasma surface, respectively.  $B(a)$  is magnetic field at the plasma surface, and  $B_{pa}$  is estimated from plasma current,  $I_p$  ( $B_{pa} = \mu_0 I_p / (2\pi a)$ ).  $B_{ta}$  is toroidal magnetic field at the plasma surface. The power supply of the toroidal field coil for the PPCD consists of six groups of capacitor bank. The timing and charging voltage of each capacitor bank is optimized to give the PPCD duration as long as possible. Typical waveform of the toroidal magnetic field outside of the wall,  $B_{\text{tout}}$ , is shown in FIG. 1 a). The plasma current is 300 kA at the flattop phase (just before the PPCD). The  $B_{\text{tout}}$  is almost constant during the discharge in the standard discharge (red line). During the PPCD, the  $B_{\text{tout}}$  is stepped down 6 times (blue line), and total flux decreases smoothly. For the standard discharge, the  $E_{\parallel}$  is usually negative during ramp up phase and more or less zero during flattop phase ( $t = 20 \sim 40$  ms) as shown by the red line in FIG. 1 b). The decrease of the total flux induces the poloidal electric field.  $E_{\parallel}$  increases rapidly and becomes positive as shown in FIG. 1 b) (blue line). The positive  $E_{\parallel}$  assists self-organization of the effective electromotive force parallel to the average magnetic field, so dynamo activity is reduced when  $E_{\parallel}$  is positive.

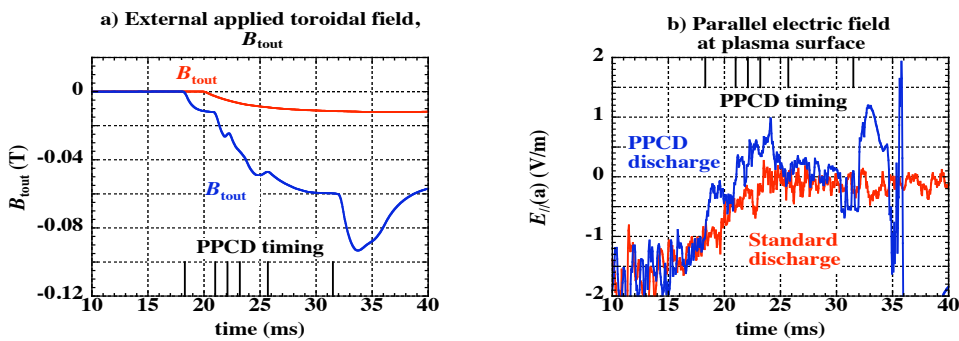


FIG. 1. Typical waveform of the toroidal magnetic field at outside of the wall,  $B_{\text{tout}}$  a) and the parallel electric field,  $E_{\parallel}$  b). The  $E_{\parallel}$  increases rapidly and becomes positive.

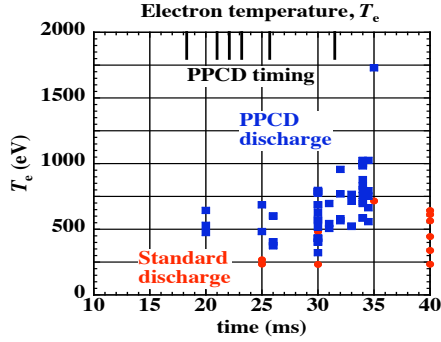


FIG. 2. The time evolution of the  $T_e$  at plasma center. Red symbols indicate the  $T_e$  for the standard discharge and the blue symbols indicate the  $T_e$  for the PPCD.

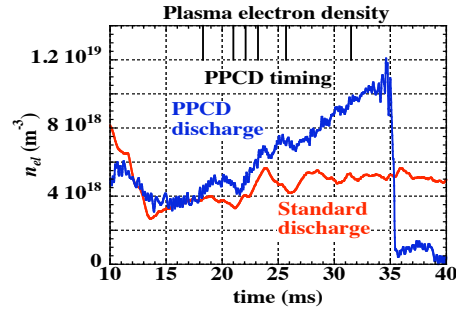


FIG. 3. The line averaged plasma electron density,  $n_{el}$  in the standard discharge (red line), and in the PPCD discharge (blue line).

By applying the PPCD, soft X-ray signal increases and reaches to a ten times higher amplitude than that in the standard discharge. A single point Thomson scattering system has been installed in TPE-RX in order to measure the electron temperature,  $T_e$ . The Thomson scattering system consists of a single pulse Nd-Yag laser, and the time evolution of the  $T_e$  is measured in a shot by shot manner [2]. FIG. 2 shows time evolution of the  $T_e$  at plasma center measured by changing the laser timing. Red symbols indicate the  $T_e$  for the standard discharge and the blue symbols indicate the  $T_e$  for the PPCD. The ensemble-averaged  $T_e$  for the standard discharge is about 428 eV at the flat top phase. The plasma density is low and the S/N ratio is bad in the standard discharge, and then few data is available at  $t = 35$  ms. However, the confinement property in standard discharge is almost constant at the flat top phase. The  $T_e$  increased rapidly during the PPCD, and ensemble-averaged  $T_e$  increased to 834 eV at the end of the PPCD. The maximum  $T_e$  became more than 1.5 keV. The electron density profile was measured using a double-chord CO<sub>2</sub>/HeNe laser interferometer, whose impact parameters normalized by  $a$  are 0.0 and 0.69 [10]. The line averaged plasma electron density,  $n_{el}$  in standard discharge was about  $5 \times 10^{18} \text{ m}^{-3}$  as shown in FIG. 3 (red line). The  $n_{el}$  in PPCD discharge was gradually increasing during the PPCD period and increased up to  $1 \times 10^{19} \text{ m}^{-3}$  at the end of the PPCD (blue line). The increases of  $T_e$  and  $n_{el}$  indicate that the confinement properties are improved by applying the PPCD. The time variations of  $\beta_p$  defined as  $2\langle n_{el}(r)T_e(r) \rangle / (B_{pa}^2 / 2\mu_0)$  are plotted in FIG. 4. Here we assume the temperature profile as  $T_e(r) = T_e [1 - (r/a)^2]$  and density profile as  $n_{el}(r) = n_0 [1 - (r/a)^4] [1 + A(r/a)^4]$ .  $n_0$  and  $A$  are determined by fitting the two measured chord values. Since the number of measured  $T_i$  values is not enough,  $T_i$  is assumed to be equal to  $T_e$  in the estimation shown in FIG. 4. The  $\beta_p$  in the standard shot is about 5% and is almost constant during the flat top phase as shown by red symbols in FIG. 4. The  $\beta_p$  increases gradually during PPCD as shown by blue symbols, and

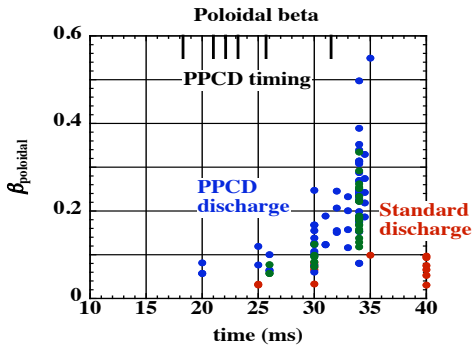


FIG. 4. The time variations of  $\beta_p$ . In PPCD discharge,  $\beta_p$  increases up to 40 %.

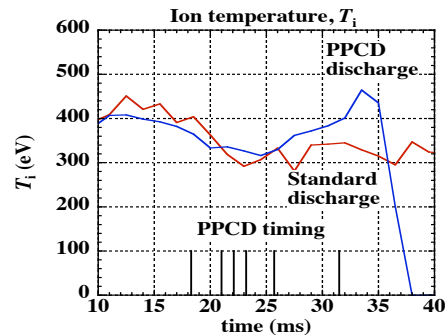


FIG. 5. Ion temperature increases after 25 ms, and reaches up to 450 eV in the PPCD discharge (blue line).

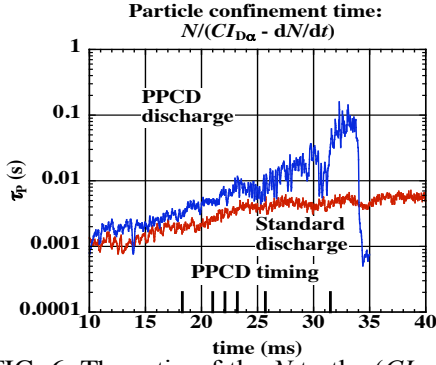


FIG. 6. The ratio of the  $N$  to the  $(CI_{D\alpha} - dN/dt)$ , which corresponds to the particle confinement time.

the ensemble-averaged  $\beta_p$  is 30% at  $t = 34$  ms. High  $\beta_p$  up to 50% was obtained at the end of PPCD. However, it should be noted that the ion pressure is assumed to be equal to the electron pressure in the above estimation. In several PPCD shots, the ion temperature is measured by the neutral particle analyzer. The  $T_i$  in the standard discharge is about 300 eV at  $t = 35$  ms as shown in FIG. 5. The peak value of  $T_i$  in the PPCD discharge is about 450 eV. Several values of  $\beta_p$  calculated by using these  $T_i$  values (then  $\beta_p$  is given by  $\langle n(r)(T_e(r) + T_i(r)) \rangle / (B_{pa}^2 / 2\mu_0)$ ) are also shown by green symbols in FIG. 4. Then the maximum  $\beta_p$  value is reduced to about 30%. Here, we note that the temperature profile used in this estimation is narrower than that observed in other large RFP device [6], so that if this is also the case in TPE-RX, the  $\beta_p$  in TPE-RX will be higher than the presently estimated value. Particle confinement time is also estimated from the total D-alpha emission,  $I_{D\alpha}$ . The D-alpha line monitors are installed at 13 of 16 port sections equally distributed around the toroidal direction of TPE-RX. The  $I_{D\alpha}$  is estimated from the summation of toroidal D-alpha line intensity distribution. The  $I_{D\alpha}$  is almost proportional to the amount of recycling deuterium from the first wall. FIG. 6 shows the ratio of the total number of electrons  $N$  to the  $(CI_{D\alpha} - dN/dt)$ , which corresponds to the particle confinement time,  $\tau_p$ . Here, the  $C$  is the relative variation of the number of ionization events per photon of the D-alpha line. In order to estimate the  $N$ , we used the electron density profile as described above. The  $\tau_p$  is almost constant after  $t = 23$  ms in the standard discharge as shown by red line in FIG. 6.  $I_{D\alpha}$  decreases one-tenth during 2~3 ms at the end of the PPCD and the  $\tau_p$  significantly increases up to ten times longer compared with that in the standard shot as shown by blue line in FIG. 6. However, we note that intensity of the  $I_{D\alpha}$  is almost observation limit during 2~3 ms at the end of the PPCD and the  $\tau_p$  might be over estimated at this period. We define the period when the  $I_{D\alpha}$  decreases and the particle confinement increases as the period of the ICR.

### 3. Magnetic turbulence and its effect on particle confinement

The reduction of the so-called Locked mode (phase-locking and wall-locking) and the high  $\Theta$  effect are important roles of the PPCD. The D-alpha emission at the place where the Locked mode

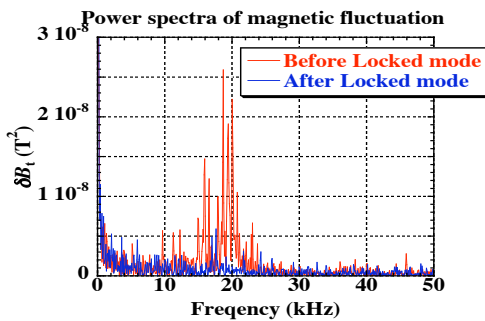


FIG. 7. The typical power spectra of the  $\delta B_1$  measured by the CEP before the Locked mode appears (red line) and after the Locked mode appears (blue line).

exists is usually higher than the other place. During the ICR, the MHD activity is reduced by the PPCD and the Locked mode disappears. However, in the pre-ICR (before the ICR), the difference of the toroidal averaged D-alpha emission between the value including the locked position and that excluding the locked position is about 15%. The difference does not significantly affect to the  $\tau_p$  within the experimental errors [4]. The reduction of the D-alpha emission is not only around the locked position, but also everywhere in the torus. The toroidally integrated D-alpha emission is reduced by 75% during the ICR, which indicates that

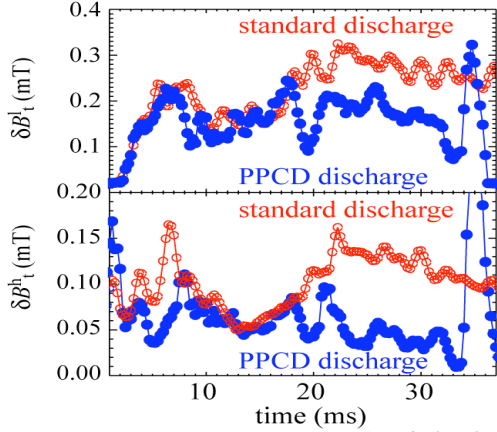


FIG. 8. Root mean square (rms) of the low frequency (5-50 kHz) magnetic fluctuation,  $\delta B_t^l$  and of the high frequency (>50 kHz) magnetic fluctuation,  $\delta B_t^h$ .

measurement using the CEP.

An extensive magnetic measurement system, MMS installed in TPE-RX [12] were the powerful tool for the measurement of the magnetic fluctuations e.g. the Locked mode phenomena. However, the MMS is installed at the outside of the vacuum vessel, and so the fast magnetic fluctuations are shielded by the vacuum vessel and cannot be observed in the MMS. In the MMS measurement, the Locked mode suddenly appears in the middle of discharge under certain discharge conditions of TPE-RX. FIG. 7 shows the typical power spectra of the  $\delta B_t$  measured by the CEP before (red line) and after (blue line) the Locked mode appears. A range of 10-30 kHz fluctuations is dominant of the CEP signals before the Locked mode appears, and decreases when the modes lock to the wall and the rotation of the tearing mode is slowing down. The low frequency signal of the MMS increases instead of the fast CEP signals after the Locked mode appears [4]. The amplitude of the MMS signal just after Locked mode appearance is similar to that of the CEP just before the Locked mode appearance. This indicates that the rapid increase of the fluctuation signal in the MMS just after the LM occurrence is the seeming one, which is not caused by the growth of the fluctuation but by the slowing down of the mode rotation (fluctuating frequency drop). It is probable that the signals with the frequency range of 10-30 kHz are correlated with the tearing mode rotation [4]. FIG. 8 shows root mean square (rms) of the low frequency (5-50 kHz,  $\delta B_t^l$ ) and high frequency (>50 kHz,  $\delta B_t^h$ ) parts of the magnetic fluctuation measured by the CEP, where the low frequency part includes the tearing mode rotation. The red color indicates the

the elimination of the Locked mode is not the main cause of the  $\tau_p$  enhancement [4]. The controlled operation in the high  $\Theta$  regime e.g. the improved high theta mode (IHTM) can have the improved plasma confinement [11]. During the PPCD, the  $\Theta$  is controlled and is becoming higher continuously, and the final  $\Theta$  is higher than the IHTM. The  $\tau_p$  measured at the comparable  $\Theta$  in the PPCD far exceeds than that in the IHTM. Therefore, the enhancement of the  $\tau_p$  by applying the PPCD cannot be simply ascribed to pinch effect [4]. The correlation between the magnetic and electrostatic turbulence and the particle confinement time  $\tau_p$  in standard and PPCD plasma is found by the

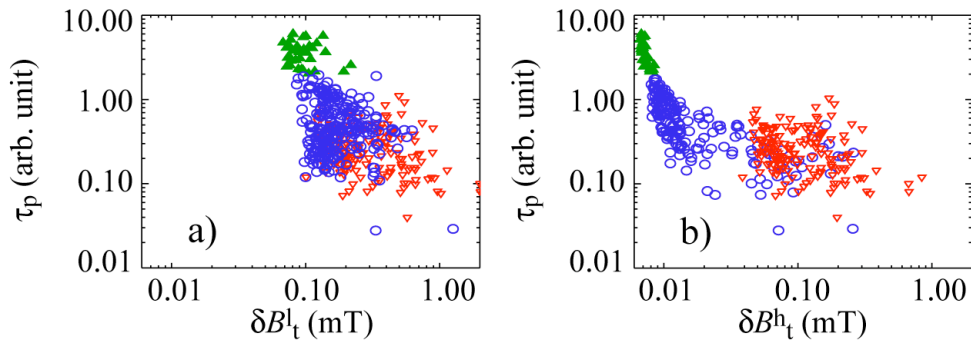


FIG. 9. Correlations between the  $\tau_p$  and the rms of the magnetic fluctuations  $\delta B_t$ . Green symbols indicate the data in the ICR, blue symbols indicate the data in the pre-ICR, and red symbols indicates the data in the standard discharge, respectively. Frame a) shows the correlation with the low frequency fluctuations and frame b) with the high frequency fluctuations.

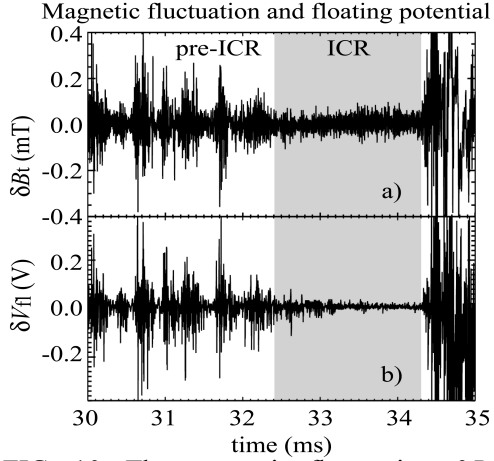


FIG. 10. The magnetic fluctuation,  $\delta B_t$  a) and the floating potential,  $\delta V_{fl}$  b) during PPCD.

case of the standard discharge, and blue does the PPCD, respectively. The PPCD starts at  $t = 18.6$  ms, and the difference between the two cases exists after that time. The magnetic fluctuations are reduced in both low and high frequency region by applying the PPCD. FIG. 9 shows the correlation between the  $\tau_p$  and the rms of the magnetic fluctuations  $\delta B_t$ . Each point in the FIG. 9 is averaged in time intervals 1ms long. Green symbols indicate the data in the ICR, blue symbols indicate the data in the pre-ICR, and red symbols indicates the data in the standard discharge, respectively. The particle confinement time has clear correlation with the both low a) and high b) frequency magnetic fluctuations. Different behavior between the fluctuations in the standard and ICR regime are not limited to the magnetic fluctuations amplitude only. FIG. 10 shows the magnetic fluctuation,  $\delta B_t$  and the floating potential,  $\delta V_{fl}$  during the PPCD. These fluctuations are filtered above 5 kHz to highlight the fluctuation. The  $\delta V_{fl}$  has a similar time evolution with the  $\delta B_t$ . These fluctuations are strongly reduced during the ICR as shown by hatching region in FIG. 10. It is shown that the fluctuations in the standard discharge are characterized by an intermittent behavior and a non-self-similar nature, but the fluctuation during the ICR in the PPCD is characterized by the self-similar nature [13,14]. To study this, we use the statistical analysis of the probability distribution function (PDF). We analyze the scaling behavior of the stochastic variable  $\Delta_\tau b(t) = \delta B_t^h(t)/\sigma_B - \delta B_t^h(t + \tau)/\sigma_B$ , which presents the characteristic fluctuations across turbulent structure at the time scale  $\tau$ . Where  $\sigma_B$  is the standard deviation. In a pure self-similar case, the PDF is independent of the  $\tau$  and collapses to a common PDF at all scales of the  $\tau$ . The shape of the PDF starts to change with the  $\tau$  by departing from the self-similarity. The shape of the PDF is generally fitted with a stretched exponential function  $F(\Delta_\tau b) = A e^{-k|\Delta_\tau b|^\alpha}$ . In the self-similar case, this function shows  $\tau$ -scale invariance. In the ICR, high frequency magnetic fluctuations of plasma have a clear self-similar behavior since  $\alpha$  is almost independent from  $\tau$ . However, fluctuations in standard plasma have a clear non-self-similar behavior [5]. To directly investigate the correlation between the nature of the turbulence and the confinement property, we study the correlation between the shape of the PDF and the  $\tau_p$ . To estimate the self-similar properties, we have defined the coefficient  $\gamma = 1 - \alpha^{\min}/\alpha^{\max}$ , where  $\alpha^{\min}$  and  $\alpha^{\max}$  are the minimum and the maximum value of  $\alpha$  of the PDFs. When the magnetic fluctuations of plasma have a self-similar behavior, the variation of the  $\alpha$  is small and the  $\alpha^{\min}$  is almost equal to the  $\alpha^{\max}$ . Therefore, the fluctuations with  $\gamma \sim 0$  have a purely self-similar behavior and the fluctuations with  $\gamma \neq 0$  have intermittent nature. FIG. 11 shows the correlation between  $\gamma$  and  $\tau_p$  in the ICR (green symbols), in the pre-ICR (blue symbols), and in the standard discharge (red symbols). The magnetic and electrostatic fluctuation signals have been divided into time intervals 1ms long, and grouped in ensembles according to  $\tau_p$ . Then the PDFs and the  $\alpha$  have been calculated for every ensemble. We can identify three regions for both magnetic fluctuations a) and electrostatic fluctuations b). The correlation has a negative trend, while there is a plateau region to 1 ms from 0.1 ms. In the high  $\tau_p$  region,  $\gamma$  is almost zero and the fluctuations of both magnetic and electrostatic have a self-similar nature.

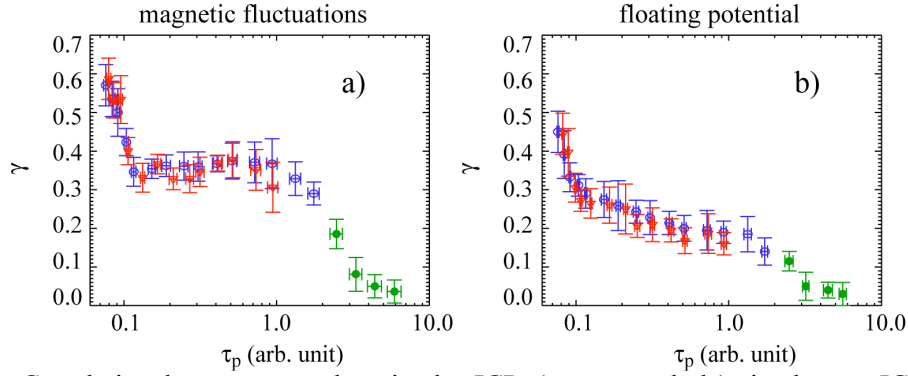


FIG. 11. Correlation between  $\gamma$  and  $\tau_p$  in the ICR (green symbols), in the pre-ICR (blue symbols), and in the standard discharge (red symbols).

#### 4. NBI experiment with single pellet injection

The first high-power and long duration NBI experiment on the RFP device was conducted. The magnetic field in RFP is generally lower than that in tokamak in more than an order, and the electron density in TPE-RX is relatively low. Both the orbit loss and the shine through due to the weak magnetic field and the low density are problem for the NBI experiment in RFP. Moreover, the diameter of the injection port is strongly limited since the scale of the port hole in the closely fitted conducting shell should be as small as possible in RFP to reduce the error magnetic field produced by the port hole. Therefore, the NBI system with a high power density (small diameter) beam in the relatively low beam energy region (less than 30 keV) is required for the RFP device. We successfully developed the NBI system satisfying these difficult requirements [15], where the following parameters are realized, the beam diameter is 36 mm around the focal point, peak maximum output power is  $\sim 1.4$  MW and power density is  $\sim 1.35$  GW/m<sup>2</sup> at the focal point. In the following NBI experiments, total input power up to 1.2 MW using 2 sets of NBI devices was injected into the plasma from the radial direction on the equatorial plane. FIG. 12 shows results of the NBI into the PPCD plasma in RFP with and without a pellet injection, a)  $n_{el}$ , b)  $I_p$ , and c) soft X-ray signal ( $I_{SX}$ ). The black dot line shows the case of PPCD, and the red dot line shows PPCD + NBI without pellet, green broken line shows PPC + pellet without NBI and blue solid line shows PPCD + NBI + pellet, respectively. Almost no effect can be observed in the case of PPCD + NBI without pellet, probably due to the long slowing down time and the beam shine through. A single ice pellet injection during the PPCD could achieve a high-density state, which contributed to the realization of high beta [3, 16]. After the pellet injection,  $n_{el}$  rapidly increased, and this regime was maintained till the end of PPCD period as shown by the green line in FIG. 12 a). The  $T_e$  and the  $I_{SX}$  signal in the case of PPCD + pellet were lower than in the case of PPCD without the pellet, but  $\beta_p$  remains almost the same because  $n_{el}$  was higher with a pellet. It is expected that the slowing down time and the beam shine through are reduced by the pellet injection during the PPCD. The blue line indicates the case of PPCD + pellet + NBI. Significant increases in  $I_p$  and  $I_{SX}$  signals

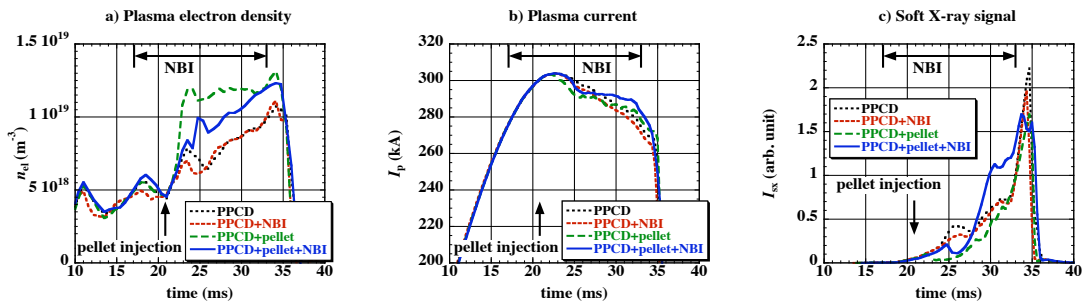


FIG. 12. a)  $n_{el}$ , b)  $I_p$ , and c) Soft X-ray emission for the NBI experiment to PPCD.

## EX/P5-25

were observed. The effective  $Z$  becomes low after the pellet injection, because the pellet injection can increase the electron density and reduce the plasma-wall interactions. Therefore, it is expected that main contribution for the increase of  $I_{SX}$  comes from the increase of  $T_e$ . Moreover the reductions of loop voltage and  $m = 0$  magnetic fluctuations were found, which also indicates the increase of  $T_e$  due to the NBI heating. This is the first report to show that the NBI heating using the NBI system suitable for RFP.

### 5. Summary

High  $\beta_p$  is obtained by applying the PPCD in the RFP experiment on TPE-RX. The  $T_e$  increases up to 1.5 keV, and the  $\beta_p$  increases to 30% from 5% during the PPCD. The plasma density increases twice as high as the standard discharge and D-alpha emission decreases to one-tenth during the PPCD. By applying the PPCD, tearing modes are stabilized, core magnetic stochasticity is reduced and hence the confinement is enhanced. We also showed that the increase in  $\tau_p$  is well correlated with the change of the magnetic and electrostatic turbulence nature. Powerful neutral beam injection experiment shows the significant increase in soft X-ray signal and plasma current by the injection into the high density RFP plasma obtained by the PPCD with the pellet injection.

### Acknowledgement

The authors are grateful to the MST group (Professor S. Prager, Dr. D. J. Den Hartog and Dr. R. O'Connell) for their valuable support and assistance in the Thomson scattering measurement. We also thank Dr. T. Hatae of JAEA for his help in calibrating the Thomson scattering system. This work was financially supported by the Budget for Nuclear Research of the Ministry of Education, Culture, Sports, Science and Technology, Japan on the basis of screening and counseling by the Atomic Energy Commission. The authors also acknowledge the support of the European Communities under the contract of the Association between EURATOM/ENEA. The views and opinions expressed herein do not necessarily reflect those of the European Commission.

### References

- [1] Y. Yagi, *et.al.*, Fusion Eng. Des. **45**, 409 (1999).
- [2] H. Koguchi *et.al.*, Plasma and Fusion Research **2**, pp. 050, (2007).
- [3] H. Koguchi *et.al.*, submitted to Plasma and Fusion Reseach.
- [4] K. Yambe *et.al.*, Jpn. J. Appl. Phys. **46**, No. 10A, pp. 6831, (2007).
- [5] L. Frassinetti *et.al.*, Plasma Phys. Control. Fusion **49**, pp. 199, (2007).
- [6] J. S. Sarff, *et.al.*, Phys. Rev. Lett. **72**, 3670 (1994).
- [7] D. J. Den Hartog, *et.al.*, Proc. 21st IAEA Fusion Energy Conference, (Chengdu, China 2006) EX/8-2.
- [8] H. Koguchi, *et.al.*, *ibid.*, EX/P3-8.
- [9] S. Martini, *et.al.*, *ibid.*, EX/7-3.
- [10] A. Canton, *et.al.*, Plasma Phys. Control. Fusion **46**, 23 (2004).
- [11] Y. Hirano, *et.al.*, Nucl. Fusion **36**, 721 (1996).
- [12] Y. Yagi, *et.al.*, Fusion Eng. Des. **46**, 47 (1999).
- [13] V. Carbone, *et.al.*, Phys. Plasmas **7**, 445 (2000)
- [14] L. Marrelli, *et.al.*, Phys. Plasmas **12**. 030701 (2005)
- [15] H. Sakakita, *et.al.*, Proc. 21st IAEA Fusion Energy Conference, (Chengdu, China 2006) FT/P5-2.
- [16] H. Koguchi, *et.al.*, Jpn. J. Appl. Phys. **45** (42), L1124 (2006).